Model of a Squirrel Cage Induction Machine with Interbar Conductances

Christian Kral Anton Haumer Bernhard Kubicek Oliver Winter
Austrian Institute of Technology
Giefinggasse 2, 1210 Vienna, Austria

Abstract

Conventional models of squirrel cage induction machines do not consider interbar currents. For the accurate numerical investigation of electrical rotor asymmetries interbar currents have to be modeled. A mathematical model of such a machine with interbar conductances is presented in this paper. An approach for the parametrization of the interbar conductances is introduced and discussed.

Keywords: Squirrel cage induction machines, electrical rotor asymmetries, interbar currents, machine model

1 Introduction

The electric conductors in the squirrel cage of an induction machine – the rotor bars and end rings – are usually either made of copper or aluminum. For die cast rotors the conducting material is not electrically insulated from the sheet iron due to the casting process. Even if copper and aluminum have a much greater electric conductivity than the sheet iron, some fractions of the rotor currents may flow through the rotor teeth, directly from bar to bar.
In mains supplied induction machines the rotor bars are usually *skewed*, i.e., the bars are twisted in tangential direction (Fig. 1 and 2) . Due to the skewing of the rotor bars the following effects occur:

1. Torque saddle points due to harmonic magnetic field waves can be avoided [1–3]

2. The torque speed characteristic and performance of the machine changes [4, 5]

3. Axial pull of the rotor caused by the tangential component of the bar currents

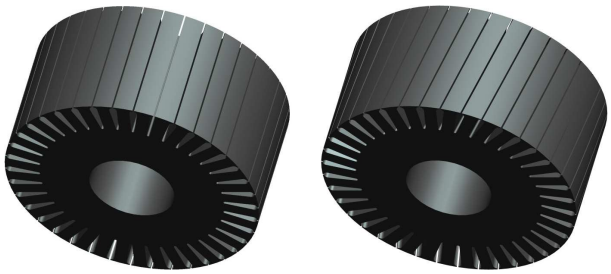

(a) unskewed rotor sheets (b) skewed rotor sheets

Figure 1: Rotor core of an induction machine

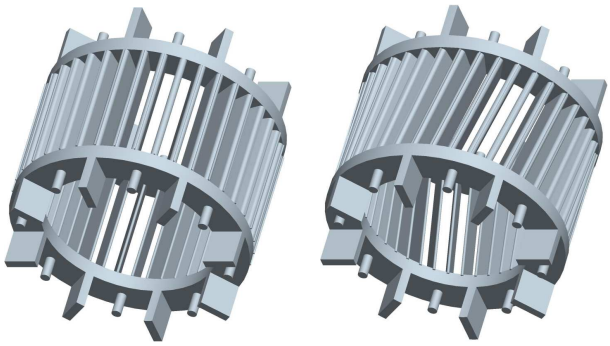

(a) unskewed cage (b) skewed cage

Figure 2: Squirrel cage of an induction machine, consisting of rotor core and a skewed or unskewed cage (bars and end rings)

4. Currents are flowing from bar to bar through the sheet iron – the so called *interbar currents*

Interbar currents significantly arise in the case of broken rotor bars or end ring segments. The intermittence of the electric conductance of either a bar or end ring segment causes the current to flow through alternative paths – in the sheet iron from bar to bar.
For the numerical investigation of interbar currents in squirrel cage induction machines finite element methods are usually applied [6–8]. Alternatively, models based on equivalent circuits can be developed to investigate the operational behavior of machines with inter-

bar currents. In such models the skewing of rotor bars can be considered by means of skewing factors applied to the calculation of the mutual inductances between stator and rotor [9, 10]. Interbar currents of electrically asymmetrical rotor cages are yet more complex to model since the rotor has to be discretized in axial direction. A Modelica model considering such axial discretization is presented in this paper. To be more precise: the presented model takes interbar conductances into account which in turn conduct the interbar currents.

2 Model Structure

The proposed induction machine model with interbar currents is derived from the *ExtendedMachines* library which was presented in [11]. The *ExtendedMachines* library includes a model of the stator and rotor winding topology, core, friction and stray-load losses, an air gap model and thermal connectors for the coupling with a thermal model or environment. From this library the air gap, cage and winding function models are extended and modified such way that an axial discretization including interbar conductances is modeled.

A diagram of the proposed machine model is depicted in Fig. 3. The stator network considers the stator resistance (`rs`), the stator stray inductance (`lssigma`) and the air gap model (`airgap`), which can be seen as electromechanical power converter. Stray-load losses (`strayLoad`), core losses (`coreStray` and `coreTerminal`, respectively, for alternate use, depending on the model character) and friction losses (`friction`) are also taken into account. On the rotor side a multiphase squirrel cage (`cage`) is modeled. Each leg of the rotor phases has to be grounded (`ground`). Stator and rotor inertia (`intertiaStator`, `inertiaRotor`) are connected with the air gap model and the shaft end (`flange`) and housing (`support`) connector, respectively.

Any symmetric or asymmetric stator winding topology (`windingStator`) can be considered by specifying the location of the begin and end of each turn – for each phase. Details about the modeling of the stator winding topology are explained in [11]. The topology of the rotor cage is fully symmetrical and formed of the periodic structure of bars and end rings as depicted in Fig. 2. Electrical rotor asymmetries are model by modified rotor bar and end ring resistances. The topology model of the squirrel cage is presented in section 3.

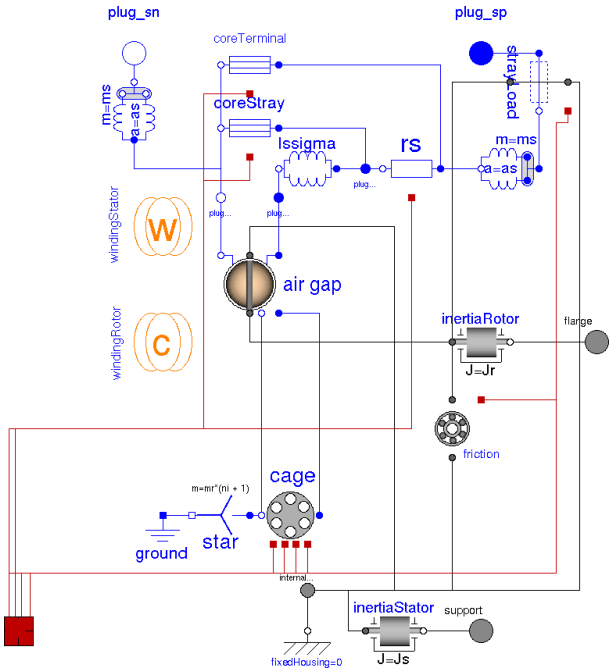

Figure 3: Modelica diagram of the proposed induction machine with interbar conductances

3 Cage Model

The presented cage model (`cage`) takes skewed rotor bars and interbar conductances into account. The interbar conductances are modeled in such a way, that each rotor bar is axially discretized and each intermediate node of two adjacent bars is connected by an an interbar conductance. A sketch of the rotor network model is presented in Fig. 4. This modeling approach does not consider current paths through the rotor yoke [12], which seems to be a reasonable simplification.

The voltages induced in the rotor meshes are calculated in the air gap model which is presented in section 4. These induced voltages are the terminal voltages $v_{[m]}$ of the cage model in Fig. 3. The currents associated with the multiphase ports of the cage model, $i_{[m]}$, are rotor mesh currents.

The cage consists of N_r rotor bars and thus N_r is also the number of end ring segments on both sides – the drive end (index a) and the non drive end (index b). In axial direction each rotor bar is subdivided into $n_i + 1$ segments. The rotor bar segments are tangentially connected by interbar conductances $G_{i[m]}$. In axial direction the rotor is thus modeled by n_i interbar conductors. Each of these conductors represents the conductance of the sheet iron including the contact conductance. Due to this structure the rotor cage consists of $(n_i + 1)N_r + 1$ elementary meshes, which are indicated

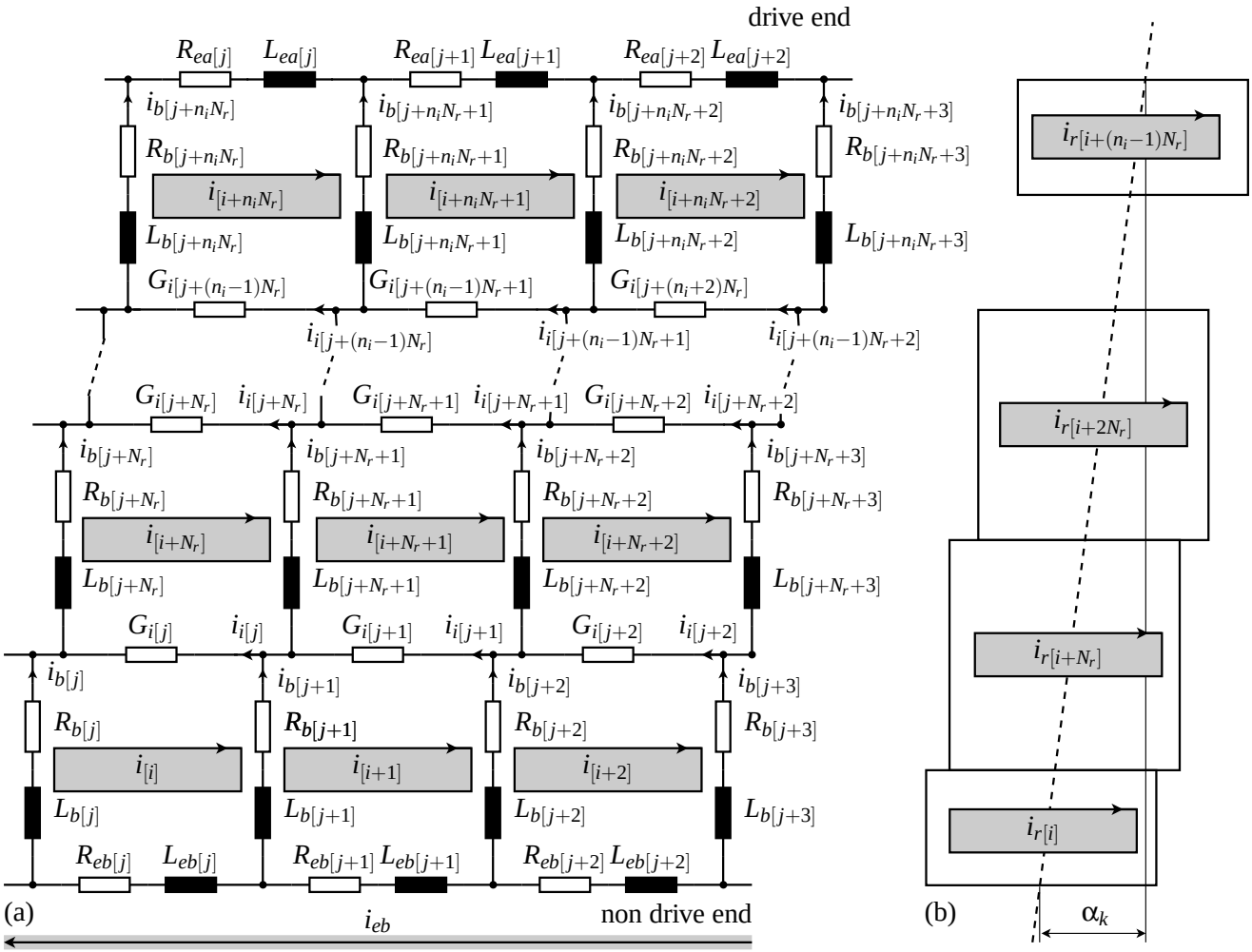

Figure 4: (a) Equivalent circuit of rotor cage with interbar conductances; (b) location of size of skewed rotor loops, skewing angle α_k

in gray in Fig. 4. For these elementary meshes the voltage equations have to be modeled.

The rotor voltage equation of the elementary mesh along the end ring on the non drive end yields

$$0 = \sum_{m=1}^{N_r} \left(R_{eb[m]}(i_{[m]} + i_{eb}) + L_{eb[m]} \frac{\mathrm{d}(i_{[m]} + i_{eb})}{\mathrm{d}t} \right). \tag{1}$$

From the remaining rotor meshes two different types of meshes have to be distinguished. An *end ring mesh*, is formed by one end ring segment, two bar segments and one interbar conductance. An *intermediate mesh* is formed of two bar segments and two interbar conductances. The indices of the meshes and the currents, respectively, are numbered in ascending order from left to right and from the non drive end to the drive end.

The rotor voltage equations for the end ring meshes of the non drive end are

$$\begin{aligned} 0 = {} & v_{[m]} + R_{b[m]} i_{b[m]} + L_{b[m]} \frac{\mathrm{d}i_{b[m]}}{\mathrm{d}t} \\ & - R_{b[m+1]} i_{b[m+1]} - L_{b[m+1]} \frac{\mathrm{d}i_{b[m+1]}}{\mathrm{d}t} \\ & + R_{eb[m]}(i_{[m]} + i_{eb}) + L_{eb[m]} \frac{\mathrm{d}(i_{r[m]} + i_{eb})}{\mathrm{d}t} - \frac{i_{i[m]}}{G_{i[m]}}, \end{aligned} \tag{2}$$

for $m \in [1, 2, \ldots, (n_i + 1)N_r]$.

For the intermediate meshes the voltage equations are

$$\begin{aligned} 0 = {} & v_{[m]} + R_{b[m]} i_{b[m]} + L_{b[m]} \frac{\mathrm{d}i_{b[m]}}{\mathrm{d}t} \\ & - R_{b[m+1]} i_{b[m+1]} - L_{b[m+1]} \frac{\mathrm{d}i_{b[m+1]}}{\mathrm{d}t} \\ & - \frac{i_{i[m]}}{G_{i[m]}} + \frac{i_{i[m-N_r]}}{G_{i[m-N_r]}}, \end{aligned} \tag{3}$$

for $m \in [N_r + 1, N_r + 2, \ldots, n_i N_r]$.

The remaining end ring meshes on the drive end are

$$\begin{aligned}0 &= v_{[m]} + R_{b[m]} i_{b[m]} + L_{b[m]} \frac{\mathrm{d}i_{b[m]}}{\mathrm{d}t} \\ &- R_{b[m+1]} i_{b[m+1]} - L_{b[m+1]} \frac{\mathrm{d}i_{b[m+1]}}{\mathrm{d}t} \\ &+ R_{ea[m-n_i N_r]} i_{[m]} + L_{ea[m-n_i N_r]} \frac{\mathrm{d}i_{[m]}}{\mathrm{d}t} + \frac{i_{i[m-N_r]}}{G_{i[m-N_r]}}, \quad (4) \\ &\text{for } m \in [n_i N_r + 1, n_i N_r + 2, \ldots, (n_i+1) N_r].\end{aligned}$$

For the interbar currents the following equations

$$i_{i[j]} = i_{[j+N_r]} - i_{[j]} \quad (5)$$

apply for $j \in [1, 2, \ldots, n_i N_r]$. Additionally, the bar currents and the mesh currents are related by

$$i_{b[j]} = i_{[j+1]} - i_{[i+N_r]} \quad (6)$$

$$i_{b[i+k]} = i_{[i+k]} - i_{[i+k-1]} \quad (7)$$

and $j = N_r(n-1)$ with $n \in [1, 2, \ldots, n_i + 1]$, and $k \in [2, 3, \ldots, N_r]$.

4 Air Gap Model

In the air gap model (`airgap`) the magnetic coupling of the m_s phase stator winding and the N_r phase rotor cage (or winding) is modeled. Due to the axial segmentation of the rotor bars, the air gap model and the cage model are coupled through a multiphase connector with $(n_i+1)N_r$ phases. The magnetic coupling between the windings of the stator and rotor is determined by the respective number of turns and the actual location of the turns with respect to each other. The relationship between the induced stator voltages, $v_{s[l]}$, and the induced rotor voltages, $v_{r[m]}$, and the respective currents $i_{s[l]}$ and $i_{r[m]}$ is expressed by

$$v_{s[j]} = \sum_{l=1}^{3} L_{ss[j,l]} \frac{\mathrm{d}i_{s[l]}}{\mathrm{d}t} + \sum_{m=1}^{(n_i+1)N_{ir}} \frac{\mathrm{d}}{\mathrm{d}t} \left(L_{sr[j,m]} i_{r[m]} \right), \quad (8)$$

$$v_{r[m]} = \sum_{j=1}^{3} \frac{\mathrm{d}}{\mathrm{d}t} \left(L_{rs[m,j]} i_{s[j]} \right) + \sum_{n=1}^{(n_i+1)N_r} L_{rr[m,n]} \frac{\mathrm{d}i_{r[n]}}{\mathrm{d}t}, \quad (9)$$

where $L_{ss[j,l]}$ are the stator inductances,

$$L_{sr[j,m]} = L_{rs[m,j]} \quad (10)$$

are the mutual stator and rotor inductances, and $L_{rr[m,n]}$ are the rotor inductances of the machine.

For the stator it is assumed that the complex winding factor, $\xi_{s[j]}$, and the number of turns, $w_{s[j]}$, can be determined for each phase based on the exact topology of each phase winding [13]. For the rotor cage the number of turns is equal to one,

$$w_{r[m]} = 1 \quad (11)$$

and the complex winding factor,

$$\xi_{r[m]} = \sin\left(\frac{\pi p}{N_r}\right) e^{-\mathrm{j}2\pi p m / N_r}, \quad (12)$$

is formed of the chording factor of two adjacent rotor bars, and the tangential location of the respective rotor mesh – assuming it were unskewed. In order to consider the skewing of the rotor bars accordingly, the tangential displacement of the rotor meshes belonging to two particular rotor bars, is modeled by a complex displacement factor, $\delta_{r[m]}$. The inductances in (8) and (9) can thus be expressed as

$$L_{ss[j,l]} = L w_{s[j]} w_{s[l]} \mathrm{Re}(\xi_{s[j]} \xi^*_{s[l]}), \quad (13)$$

$$L_{sr[j,m]} = L w_{s[j]} w_{r[m]} \zeta_{r[m]} \mathrm{Re}(\xi_{s[j]} \xi^*_{r[m]} \delta_{r[m]} e^{\mathrm{j}\gamma_m}), \quad (14)$$

$$L_{rr[m,n]} = L w_{r[m]} w_{r[n]} \zeta_{r[m]} \zeta_{r[n]} \mathrm{Re}(\xi_{r[m]} \xi^*_{r[j]} \delta_{r[m]} \delta^*_{r[n]}), \quad (15)$$

where L is the base inductance of one turn with a width equal to one pole pair. In this equations the expression

$$\zeta_{r[m]} = \begin{cases} \frac{1}{2n_i} & \text{if } m \text{ refers to an end ring mesh} \\ \frac{1}{n_i} & \text{if } m \text{ refers to an intermediate mesh} \end{cases} \quad (16)$$

applies, which determines the axial length of each end ring or intermediate mesh. The axial length of each mesh is modeled such way, that two bar segments of equal length e contribute to one interbar conductor (Fig. 5). Expression (16) is also used to determine the resistances and stray inductances of the bar segments with respect to the total bar resistance and stray inductance, respectively.

In the induction machine model of Fig. 3 the winding factors of the stator winding and the rotor cage are determined by the models `windingStator` and `windingRotor`, respectively. These models compute the winding factors, number of turns, displacement factors and (16) and propagate them to the air gap model. The input parameters are the skewing angle α_k (Fig. 4), the number of phases and the remaining topology data of the stator winding.

The electromagnetic torque of the induction machine is

$$T_e = \sum_{j=1}^{3} \sum_{m=1}^{(n_i+1)N_r} \frac{\partial L_{sr[j,m]}}{\partial \gamma_m} i_{s[j]} i_{r[m]}, \quad (17)$$

and applies to the stator and rotor inertia, with inverse signs, however. In this equation γ_m indicates the electrical angle of the rotor with respect to the stator.

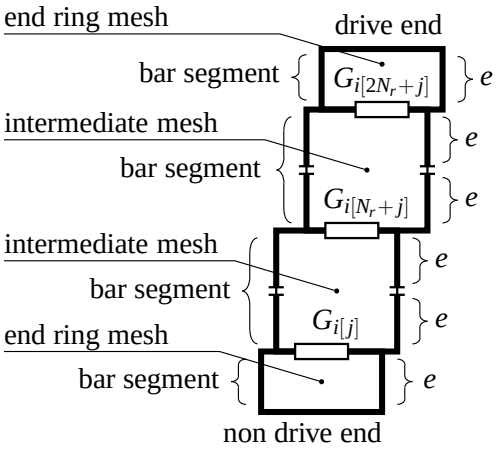

Figure 5: Sketch of two skewed rotor bars with $n_i = 3$ interbar conductances: two equal bar segments (length e) contribute to one interbar segment; this results in different bar segment lengths for end ring meshes and intermediate meshes

5 Practical Application

5.1 Model Development and Compilation

The model was developed with Dymola 6.0b and the C code was compiled in parallel on a 64 bit Linux cluster. The compilation and execution times of the models very much rely on the number of interbar segments, n_i. Two different simulations were carried out for the cases $n_i = 4$ and $n_i = 9$. For the second case a newer version of the Gnu C Compiler (GCC) had to be used in order to keep the compilation time in a reasonable range. The compilation of one model required approximately 8 GB memory and took one hour. Hence, a 64 bit GCC version was use to compile the 32 bit files. The simulation model was used in a project where 25 different machine configurations were investigated. Since the different configurations could be investigated independently the compilations and simulations were performed in parallel on different nodes on the Linux cluster.

For each model a total (real time) simulation time span of 12.5 s was performed. The cases $n_i = 4$ and $n_i = 9$ required 10 and 72 hours of CPU time, respectively. For the computation of each simulation in the project, a total of approximately 7000 hours of CPU time accumulated. During the comparison of these two cases it turned out, that $n_i = 9$ shows only a slight increase of accuracy and is not necessary for most investigations.

Figure 6: Squirrel cage rotor with respect to the configuration with one broken rotor bar (segment)

5.2 Parametrization of the Model

For the investigated project, the regular induction machine parameters were determined from a electromagnetic design tool. This way the resistances and stray inductances of the bars and end ring were calculated. The design tool does not calculate the interbar conductances, however, since these quantities very much rely on the manufacturing process and the contact conductances between the conductor and the sheet iron. In practice, the interbar resistances between two bars can usually not be measured without destroying the rotor cage [14–17].
Significant interbar currents arise in the rotor if one bar or end ring of the machine is broken. Therefore the configuration of one broken bar (Fig. 6) and one broken end ring segment (Fig. 7) are investigated. In order to compare measurement and simulations a method has to be applied which allows assessment of the effects caused by a broken rotor bar or end ring segment. Such a method is the Vienna Monitoring Method (VMM), originally introduced in 1997 [18–20]. The VMM calculates a fault indicator which is related with the fault extent. Interbar currents deteriorate the fault indicator and thus the comparison of measurement and simulation results can be used to parametrize the interbar conductances. In this context it is assumed that the interbar conductances of the entire rotor topology are equal

$$G_{i[m]} = \frac{G_{i\mathrm{ref}}}{n_i} \tag{18}$$

for $m \in [1, 2, \ldots, n_i N_r]$.
Measurement and simulations results for the two investigated configurations and $n_i = 4$ are depicted in Fig. 8:

Figure 7: Squirrel cage rotor with respect to the configuration with one broken (removed) end ring segment

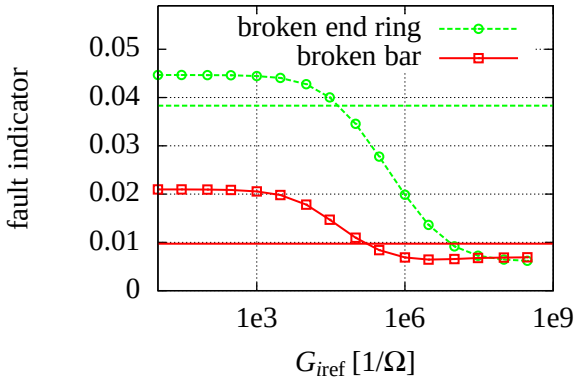

Figure 8: Fault indicator of the VMM versus interbar conductance G_{iref}

- *Broken end ring segment*: The measured fault indicator is shown as horizontal dashed line. The simulation result to match decreases with increasing total interbar conductance G_{iref}. The intersection of the simulation and measurement results indicates well parametrized simulation model.

- *Broken rotor bar*: The fault indicator obtained by measurements is depicted as horizontal solid line. The intersection of this line with the simulation result leads to a solution close to the one obtained for one broken end ring segment.

From the two intersection points of Fig. 8 an average value of $G_{\text{iref}} = 2.3 \times 10^5 \, \frac{1}{\Omega}$ is obtained, which satisfies the required accuracy of both fault configurations. If the two intersection points were much further apart, this would indicate that the simulation model is not reflecting the real machine behavior.

6 Conclusions

This paper presents a mathematical model of a squirrel cage induction machine with interbar conductances and skewed rotor bars. For this purpose each rotor bar is axially subdivided into bar sections which are tangentially connected by interbar conductors. This way a discretized rotor topology model is developed. The Modelica models including equations of the air gap and cage are presented in detail.
The simulation model was used in a project where the impact of interbar currents, in combination with electrical rotor asymmetries are studied. In order to parametrize the interbar conductances two different fault configurations are investigated by measurements and simulations. The obtained parameter of the total interbar conductance confirms that the proposed simulation model leads to reasonable results and accurately reflects real machine behavior under rotor fault conditions.

References

[1] R. Weppler, "Ein Beitrag zur Berechnung von Asynchronmotoren mit nichtisoliertem Läuferkäfig," *Archiv für Elektrotechnik*, vol. 50, pp. 238–252, 1966.

[2] J. Stèpina, "Oberwelleneinflüsse, Querströme und unsymmetrische Sättigung in der programmierten Berechnung von Einphasen-Asynchronmotoren," *Siemens-Zeitschrift*, vol. 46, pp. 819–824, 1972.

[3] J. Stepina, "Querstroeme in Kaefiglaeufern," *e&i*, vol. 92, pp. 8–14, 1973.

[4] W. Neuhaus and R. Weppler, "Einfluß der Querströme auf die Drehmomentkennlinie polumschaltbarer Käfigläufermotoren," *ETZ-A*, vol. 88,3, pp. 80–84, 1967.

[5] Y. Kawase, T. Yamaguchi, Zhipeng Tu, N. Toida, N. Minoshima, and K. Hashimoto, "Effects of skew angle of rotor in squirrel-cage induction motor on torque and loss characteristics," *IEEE Transactions on Magnetics*, vol. 45, no. 3, pp. 1700–1703, March 2009.

[6] G. H. Müller and C. F. Landy, "Finite element analysis of field distribution of squirrel cage induction motors having broken rotor bars and interbar currents," *Proceedings of the International*

Conference on Electrical Machines, ICEM, pp. 577–581, 1994.

[7] S. L. Ho, H. L. Li, and W. N. Fu, "Inclusion of interbar currents in a network- field coupled time-s tepping finite-element model of skewed-rotor induction motors," *IEEE Transactions On Magnetics*, vol. 35, no. 5, pp. 4218–4225, September 1999.

[8] Katsumi Yamazaki and Yuta Watanabe, "Interbar current analysis of induction motors using 3-d finite-element method considering lamination of rotor core," *IEEE Transactions On Magnetics*, vol. 42, no. 4, pp. 1287–1290, April 2006.

[9] G. Müller, *Elektrische Maschinen - Grundlagen, Aufbau und Wirkungsweise*, VEB Verlag Technik, Berlin, 4 edition, 1977.

[10] S.E. Zouzou, A. Ghoggal, A. Aboubou, M. Sahraoui, and H. Razik, "Modeling of induction machines with skewed rotor slots dedicated to rotor faults," *SDEMPED*, 2005.

[11] C. Kral and A. Haumer, "Simulation of electrical rotor asymmetries in squirrel cage induction machines with the extendedmachines library," *International Modelica Conference, 6th, Bielefeld, Germany*, , no. ID140, pp. 351–359, 2008.

[12] David G. Dorrell, Piotr J. Holik, Patrick Lombard, Hans-Jørgen Thougaard, and Finn Jensen, "A multisliced finite-element model for induction machines incorporating interbar current," *IEEE Transactions on Industry Applications*, vol. 45, no. 1, pp. 131–141, 2009.

[13] C. Kral and A. Haumer, "Modelica libraries for DC machines, three phase and polyphase machines," *International Modelica Conference, 4th, Hamburg, Germany*, pp. 549–558, 2005.

[14] S. Williamson, C. Y. Poh, and A. C. Smith, "Estimation of the inter-bar resistance of a cast cage rotor," *IEEE International Electric Machines and Drives Conference, IEMDC, Wisconsin, USA*, vol. 2, pp. 1286–1291, 2003.

[15] D. G. Dorrell, T. J. E. Miller, and C. B. Rasmussen, "Inter-bar currents in induction machines," *IEEE Transactions on Industry Applications*, vol. 39, no. 3, pp. 677–684, May-June 2003.

[16] D. Gersh, A. C. Smith, and A. Samuelson, "Measurement of inter-bar resistance in cage rotors," *Conference Proceedings of the Eighth International IEE Conference on Electrical Machines and Drives, EMD*, , no. 444, pp. 253–257, 1997.

[17] R. F. Walliser and C. F. Landy, "Assessment of interbar currents in double cage induction motors with broken rotor bars," *IEEE Transactions on Energy Conversion*, pp. 159–164, 1994.

[18] R. Wieser, C. Kral, F. Pirker, and M. Schagginger, "On-line rotor cage monitoring of inverter fed induction machines, experimental results," *Conference Proceedings of the First International IEEE Symposium on Diagnostics of Electrical Machines, Power Electronics and Drives, SDEMPED*, pp. 15–22, 1997.

[19] R. Wieser, C. Kral, F. Pirker, and M. Schagginger, "Rotor fault detection of inverter fed induction machines including experimental results," *Seventh European Conference on Power Electronics and Applications, EPE*, vol. 2, pp. 2532–2538, 1997.

[20] R. Wieser, C. Kral, F. Pirker, and M. Schagginger, "On-line rotor cage monitoring of inverter-fed induction machines by means of an improved method," *IEEE Transactions on Power Electronics*, vol. 14, no. 5, pp. 858–865, September 1999.